P O L S K A   A K A D E M I A   N A U K
INSTYTUT MASZYN PRZEPŁYWOWYCH

PRACE INSTYTUTU MASZYN PRZEPŁYWOWYCH

TRANSACTIONS OF THE INSTITUTE OF FLUID-FLOW MACHINERY

70-72

WARSZAWA–POZNAŃ 1976

PAŃSTWOWE WYDAWNICTWO NAUKOWE

PRACE INSTYTUTU MASZYN PRZEPŁYWOWYCH

poświęcone są publikacjom naukowym z zakresu teorii i badań doświadczalnych w dziedzinie mechaniki i termodynamiki przepływów, ze szczególnym uwzględnieniem problematyki maszyn przepływowych

*

THE TRANSACTIONS OF THE INSTITUTE OF FLUID-FLOW MACHINERY

exist for the publication of theoretical and experimental investigations of all aspects of the mechanics and thermodynamics of fluid-flow with special reference to fluid-flow machinery

REDAKCJA – EDITORIAL OFFICE
Instytut Maszyn Przepływowych PAN
ul. Gen. Józefa Fiszera 14, 80-952 Gdańsk, skr. pocztowa 621, tel. 41-12-71

Printed in Poland

PAŃSTWOWE WYDAWNICTWO NAUKOWE – ODDZIAŁ W POZNANIU

Wydanie I. Nakład 630+90 egz. Ark. wyd. 63,25 Ark. druk. 49,25 Papier druk. sat. kl. V. 65 g., 70×100. Oddano do składania 4 VII 1975 r. Podpisano do druku w czerwcu 1976 r. Druk ukończono w czerwcu 1976 r. Zam. 528/118. H-16/245.
Cena zł 190,–

DRUKARNIA UNIWERSYTETU IM. ADAMA MICKIEWICZA W POZNANIU

III KONFERENCJA NAUKOWA

na temat

TURBINY PAROWE WIELKIEJ MOCY

Gdańsk, 24 - 27 września 1974 r.

*

IIIrd SCIENTIFIC CONFERENCE

on

STEAM TURBINES OF GREAT OUTPUT

Gdańsk, September 24 - 27, 1974

*

III НАУЧНАЯ КОНФЕРЕНЦИЯ

на тему

ПАРОВЫЕ ТУРБИНЫ БОЛЬШОЙ МОЩНОСТИ

Гданьск, 24 - 27 сентября 1974 г.

PRACE INSTYTUTU MASZYN PRZEPŁYWOWYCH
1976 Zeszyt 70 - 72

HARALD B. CARRICK
Great Britain*

Calculation of End-Wall Flow in Turbine Cascades

Introduction

This paper is concerned with the application of three calculation methods to the end-wall flow in turbine cascades. Each of the methods is described, the principle assumptions reviewed and, where possible, example calculations with experimental comparisons are included.

The first two methods, following the classical approach of dividing the flow into an inviscid mainflow and a boundary layer, compute the development of the boundary layer when the mainstream flow is known; whereas the third method solves for the entire flow field.

The first, an annulus wall boundary layer method has received much development [13], [16], especially for low deflection cascades and here only brief details of the method of Lindsay [18] are reported with calculations for a guide vane and an impulse turbine cascade.

The second, starting from a three-dimensional boundary layer method for unbounded flows (Smith [25]) is developed into a method suitable for the bounded boundary layer in a blade row. Application to a turbine stator cascade is discussed.

The third, a three-dimensional inviscid calculation method due to Stuart [26] was adapted so that it could be applied to an impulse turbine cascade of moderately high aspect ratio. The method is described, the difficulties in using it recorded and some results of the calculations presented.

1. An annulus wall boundary layer method

1.1. Introduction

This theory is concerned with predicting the development of turbulent annulus wall boundary layers in turbomachines. The intended application is that of providing values of mainstream displacement, work variations and losses in the end-wall regions for use in inviscid through flow or streamline curvature calculations. Measurements in linear and annular cascades provide experimental data for comparison with the theory. For compatibility with the axisymmetric models of the mainflow (Marsh [19], Novak [22]) and

* Engineering Department, Cambridge University, Cambridge.

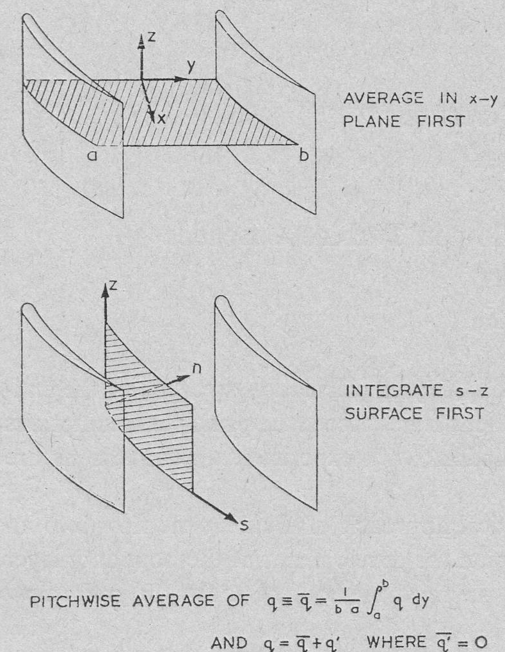

Fig. 1. Alternative methods of obtaining the momentum integral pitch-averaged boundary layer equations

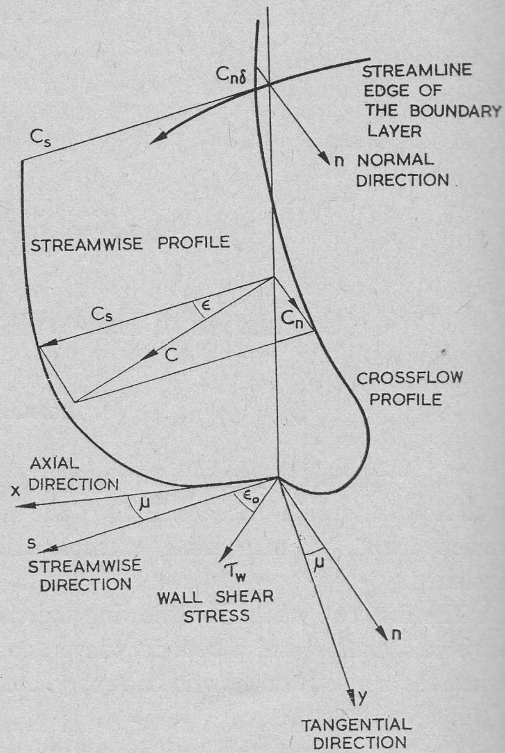

Fig. 2. Coordinate system and notation for the boundary layer

to achieve a practically desirable simplification, two-space variable equations must be used. Thus passage-averaged or axisymmetric boundary layer equations are used (Fig. 1). Additionally a momentum integral approach is followed and the equations which are solved are therefore ordinary differential equations. These methods have been the subject of much research at Cambridge and the most recent summary is that of Horlock and Perkins [16]. Some other references are [13, 15, 16, 18, 5].

1.2. The method

The details of the method presented here is that of Lindsay [18] and the equations used are given in Appendix A. Here the principle steps are noted. The coordinate system used, and the notation are illustrated in Fig. 2.

1.2.1. Passage-Averaging

All quantities in the equations of motion are written as the sum of their mean value across a pitch plus a perturbation e.g.

$$q = \bar{q} + q' \quad \text{where} \quad \bar{q} \equiv \frac{1}{b-a}\int_a^b q\,dy. \qquad \text{(Fig. 1)}$$

These equations are then either averaged across the pitch and integrated through the boundary layer to form momentum integral equations or integrated in a streamline co-ordinate system and then averaged across the pitch.

Two problems arise. The first concerns the terms involving the products of perturbations from the mean. These can be neglected if the blade loading is low. The second concerns the presence of the blades which are represented by a 'body force' or distributed pressure field in the averaged flow. This pressure field can, and must, vary with distance from the wall, unlike in an unbounded boundary layer. Secondary flow analysis is used to obtain expressions for the terms involving this variation [10, 14].

1.2.2. Physical assumptions

Additional assumptions have to be made to close the equations.

A Coles profile [3] is assumed for the streamwise velocity profile.

A conventional shear stress relation (Coles') is assumed for the wall shear stress averaged over a blade pitch.

A simple entrainment law (Head [11]) is used.

A cross-flow profile is modelled on the Johnston profile with an additional term representing the effect of the blades in restricting the crossflow. This was derived by Horlock [14] (see Fig. 3). The angle A is determined from the secondary flow analysis and the apex

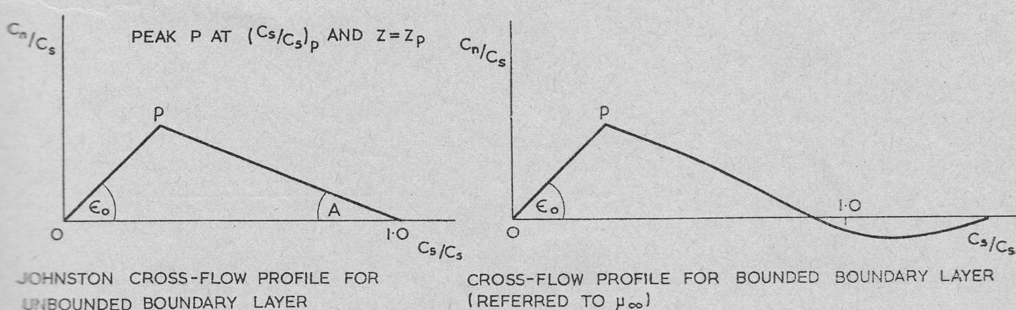

Fig. 3. Polar plots of the cross-flow profile

height is allowed to vary with its minimum value being that suggested by Johnston [17]. Thus both the streamwise and the crosswise profiles are described by two parameters; the first by c_f and Π, the second by ε_0 and z_p.

1.3. Solution procedure

Five equations are formed for the quantities: δ – the boundary layer thickness, $\varepsilon=c_\tau/C_s=\tau_w/\rho C_s^2$ – wall friction velocity ratio, Π – Coles wake factor, ε_0 – cross-flow profile parameter, z_p – cross-flow profile peak. These are integrated simultaneously by a Runge-Kutta technique which is of fourth-order accuracy.

Computation times are small, being less than two seconds for forty steps on an IBM 370/165 (10–20 points within a blade row would be typical) and storage requirements for such a run are also modest (68 k-bytes).

1.4. Results

The first calculation attempted is of a set of 52 degrees deflection guide vanes with experimental measurements performed by Gregory-Smith [9]. The mainstream velocity and flow angle (input to the calculation) are shown in Fig. 4. The computed boundary layer parameters are shown in Fig. 5, with the experimental values superimposed. As can be seen, although the method does manage to calculate through the blade row the comparison with experiment is not favourable.

The second calculation is for an impulse turbine cascade of 72 degrees deflection. This was the cascade used by Armstrong [2]; however, no boundary layer measurements are available for comparison. The input data and the computed boundary layer parameters are shown in Figs. 6 and 7.

The method has been applied successfully to cascades of low turning [16] but difficulty is expected in high turning blade rows due to the large variation in flow conditions across a pitch and the importance of extra terms in the momentum equations. This difficulty normally takes the form of the sum of the mainstream angle α and cross flow angle at the wall ε_0 approaching or attempting to exceed 90 degrees. This causes the peak shown

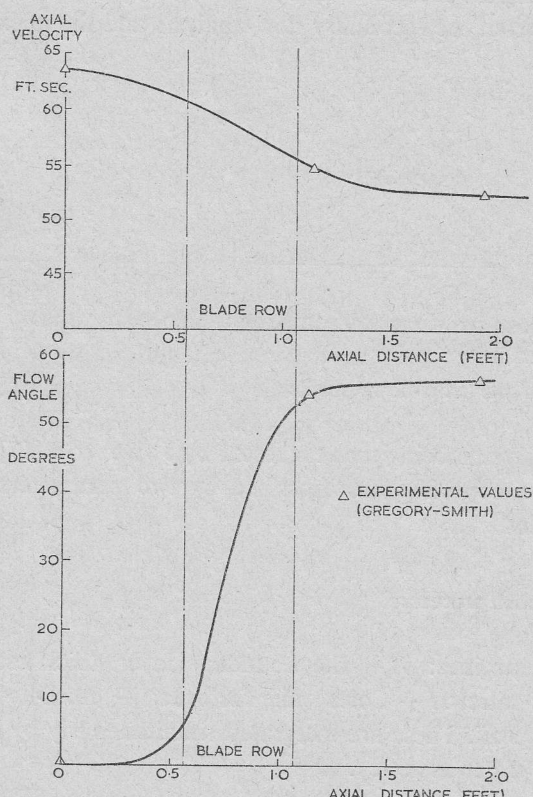

Fig. 4. Jones guide vanes — input data

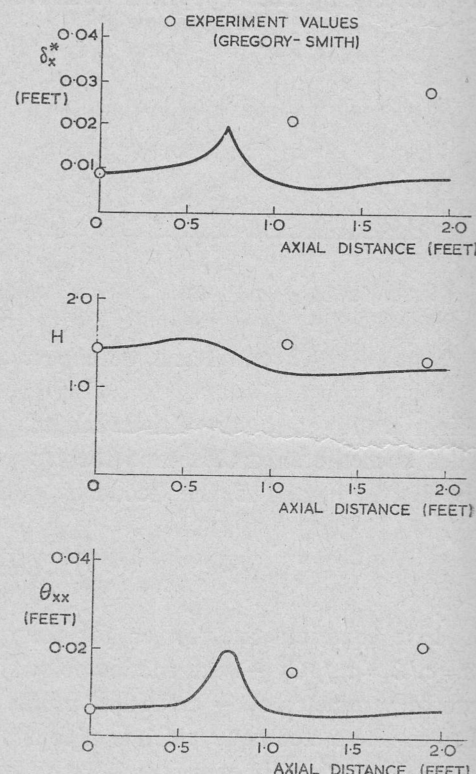

Fig. 5. Jones guide vanes — results of annulus wall boundary layer calculation

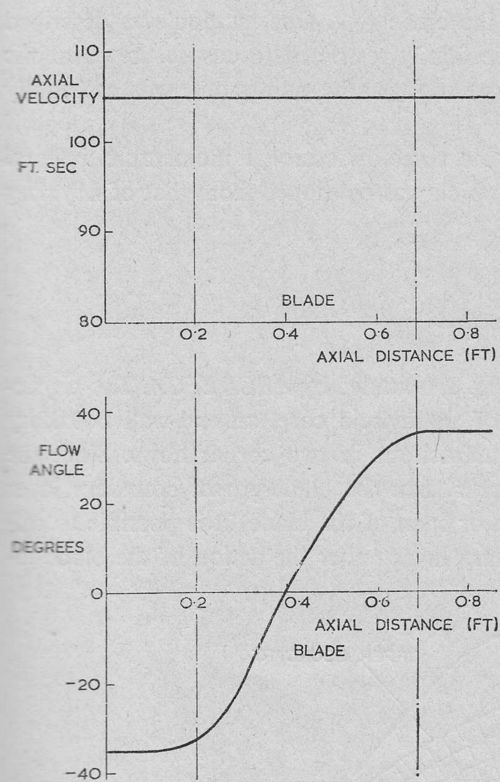

Fig. 6. Armstrong cascade – input data

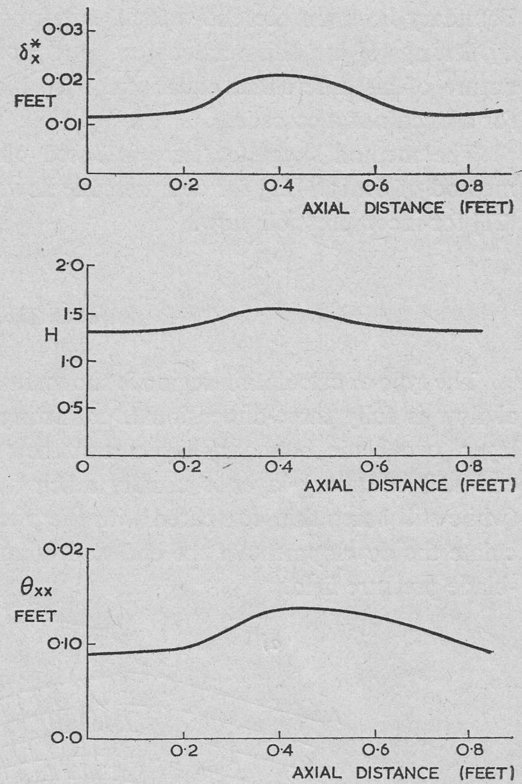

Fig. 7. Armstrong cascade – results of annulus wall boundary layer calculation

in the results of Fig. 5. If the force defect D_y (see Appendix A) becomes larger than predicted by the secondary flow analysis at high turning then this would tend to overcome this problem but the evidence to prove this contention is lacking.

2. A three-dimensional boundary-layer method

2.1. Introduction

Since in a high turning blade row there are large variations in flow quantities across a blade passage we may wish to turn to a three-dimensional boundary layer method, as suggested by Dunham [7], to provide a more detailed description of the end-wall flow than passage-averaged equations.

Such a calculation should give insight into the complex effects of inlet boundary layer thickness and turning on end-wall total pressure loss caused by the large cross-flow and thinning of the boundary layer as it is swept across the passage. It might also give an estimate of the amount of low total pressure fluid which passes onto the suction surface of the blade passage and it may provide information on the nature of the essentially new boundary layer on the end-wall at exit from the blade row. One method was described by Dring [6] but this was subject to a profile family restricted to ensure the parabolic nature of his differential equations. Also his solution, as he points out, was essentially for a duct, not a cascade.

The method suggested here is based on the three-dimensional momentum integral method of Smith [25] for compressible flow, which was developed from that of Myring [21] for incompressible flow.

2.2. The method

The type of calculation region is shown in Fig. 8, bounded by *ABCDEFGA*. The physical flow is fully three-dimensional, consisting of an inviscid core, an end-wall boundary layer, two blade boundary layers and their interactions in two corner flows. Since the end-wall boundary layer is usually much thicker than the blade-grown boundary layer (while still being thin compared with the pitch or span of the blade) it is possible to calculate the development of the end-wall boundary layer under the action of the blade-to-blade pressure field.

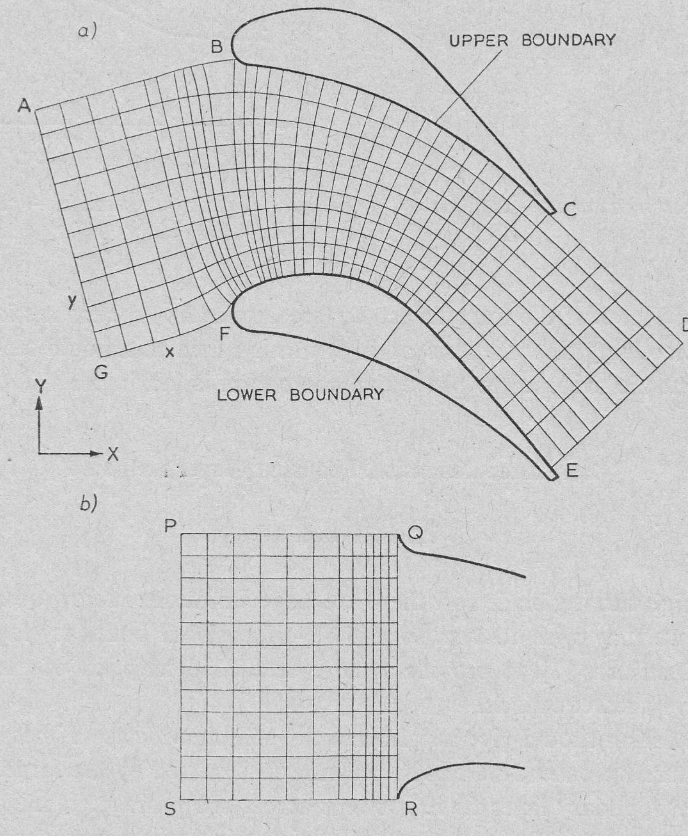

Fig. 8. Calculation region for three-dimensional boundary layer method; a) main calculation grid, b) inlet section calculation grid

The corner flows can be represented by the treatment of the boundary conditions on the pressure and suction sides of the passage (*BC*, *EF*) provided the flow out of the end-wall boundary layer is assumed to be turned onto the blade surface and any inflow is assumed to be determined by the flow towards the corner from the blade boundary layer (Fig. 9).

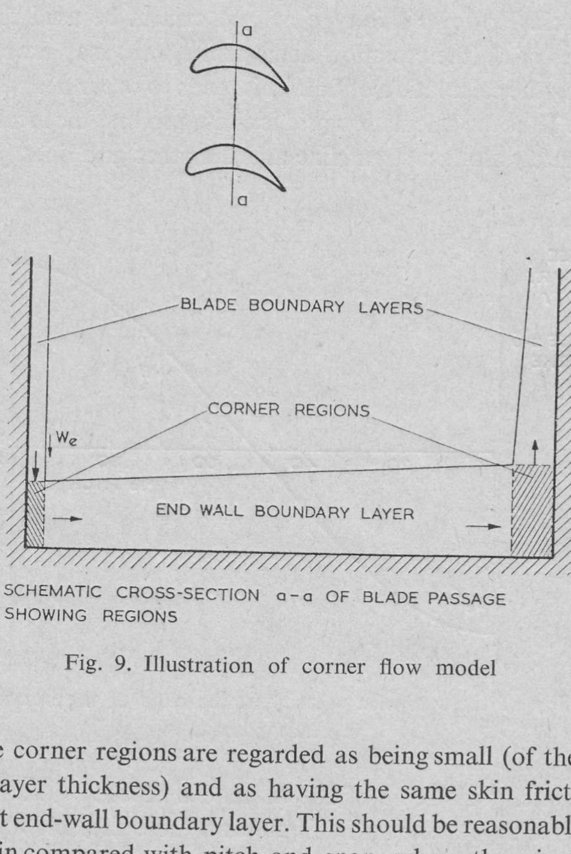

Fig. 9. Illustration of corner flow model

In this model the corner regions are regarded as being small (of the same order as the end-wall boundary layer thickness) and as having the same skin friction and other properties as the adjacent end-wall boundary layer. This should be reasonable when the end-wall boundary layer is thin compared with pitch and span, where there is no separation on the end-wall itself and where secondary flow generated by turning of the primary shearflow dominates the flow. It should be noted that this last assumption is supported by the view of Perkins [23] that the turbulence induced secondary flow will be much smaller than the secondary flow due to even small to moderate turning.

A strong flow of fluid out of the end-wall boundary layer (due to the secondary flow) is expected along *FE* and an initially weaker inflow is expected along *BC* (Fig. 8). At *FE* (the suction surface side of the passage) the outflow is allowed to take place unimpeded and is regarded, physically, as leaving the calculation region and collecting on the blade surface. At edge *BC* (the pressure surface side of the passage) the boundary layer may be assumed collateral (Dring [6]) or, preferably, the inflow can be related to the blade boundary layer (Figs. 9, 10). See 2.3.3 and Appendix B.

In the boundary layer calculation [25], the solution of the momentum integral relations, which are written in general curvilinear coordinates, proceeds by marching downstream from initial values along *AG*. Since the equations are hyperbolic in nature the numerical method takes the characteristic directions into account in evaluating derivatives. Also, boundary values must be provided along all the edges of the calculating region where characteristics enter (such as *BC*).

Conditions along the upstream boundaries must repeat due to the periodicity of the cascade and one grid on which this condition can be applied simply is that with y grid lines parallel with the pitch. However this type of grid cannot be used throughout the whole region as local values of ε_0 (the crossflow angle at the wall) may exceed the angle between the grid lines, causing the calculation of fail. This tends to occur near the leading edge or on the lower boundary. Thus the calculation grid is chosen so that the local direction of integration (x) is approximately along a streamline and the other grid lines (y) are approximately normal.

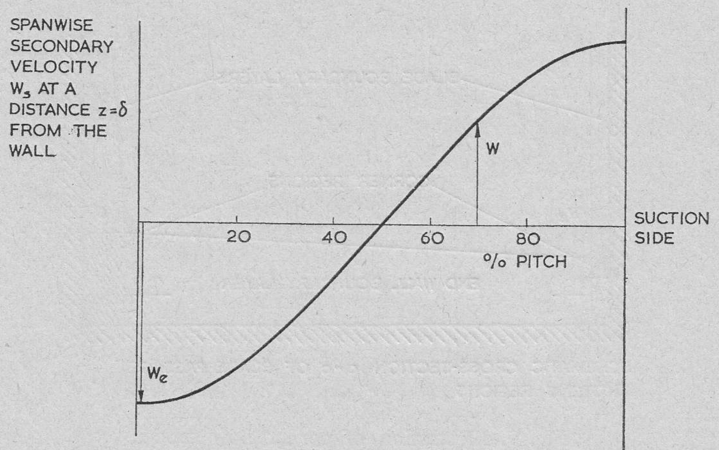

Fig. 10. Variation of the spanwise velocity at the edge of the boundary layer across a blade passage

To achieve periodicity upstream of the cascade a separate inlet section calculation is performed on the grid *PQRS* shown in Fig. 8 and here the derivatives with respect to y on the boundaries *PQ* and *RS* can be expressed in terms of the values within the region. The results of this cascade solution are then used to provide the correct boundary values for the main calculation along the edges *AB* and *GF*.

2.3. Solution procedure

The steps in the solution procedure are given briefly here. More details can be found in Appendix B.

2.3.1. Blade-to-blade potential solution

A method, such as that of Smith [24] can be used to provide the values of the free stream velocities (U, V) at all calculation points as well as the blade pressure distribution. For consistency with the secondary flow analysis of the bounded boundary layer (see section 2.2) the velocities (U, V) which apply to the midspan of the cascade $(\tan^{-1} V/U=\mu_\infty)$ should be corrected by $c_{n\delta}$, the secondary flow velocity normal to the streamline at the edge of the boundary layer. The modified velocities are V^1 and U^1, where $\tan^{-1}V^1/U^1=\mu_\delta$ and $c_{n\delta}$ can be obtained from the analysis of [14].

2.3.2. Two-dimensional blade boundary layer solution

If the boundary condition along edge BC of the channel is to be related to the blade boundary layer then a calculation must be made of the displacement thickness δ_s^* of the blade boundary layer. The method of Mellor [20] is suitable.

2.3.3. Boundary condition calculation

Using the approximate analysis of Horlock [14] the spanwise secondary velocity is estimated at the edge of the end-wall boundary layer (Fig. 10). Then, assuming approximately colateral flow in the blade boundary layer the mass flow into the corner $W_e\delta_s^*$=mass flow out of the corner$=-C_s\delta_n^*$ end wall.

2.3.4. End-wall calculation

Using the information from steps 1 and 3 above the momentum equations are integrated subject to the additional assumptions of profile form, skin friction and entrainment (see Appendix B) for the variables Θ_{11}, $\bar{H}$ and ε_0.

2.4. Results

The computer program for the P. D. Smith boundary layer procedure has been modified to include the boundary conditions detailed in 2.2 and is being applied, as a test case, to the turbine stator cascade shown in Fig. 8. The results of the blade-to-blade solution were kindly made available by Dr. D. J. Smith of the National Gas Turbine Establishment. A 36×11 grid is employed for the boundary layer calculations (11 points across the pitch) and storage requirements are 120 k-bytes with computation times of around 12 seconds on an IBM 370/165.

In Fig. 11 is shown the distribution of the parameters Θ_{11}, H, ε_0 across a pitch at three positions in the calculation. The distortion of the boundary layer caused by the blade pressure field upstream of the blade is quite considerable and it seems desirable that the cascade condition should be included. The tremendous thinning of the boundary layer which takes place has two causes: firstly the acceleration of the mainstream and secondly the secondary flow out of the boundary layer at the suction side of the passage. These are both important in this high reaction blade, but in an impulse blade the former would not occur.

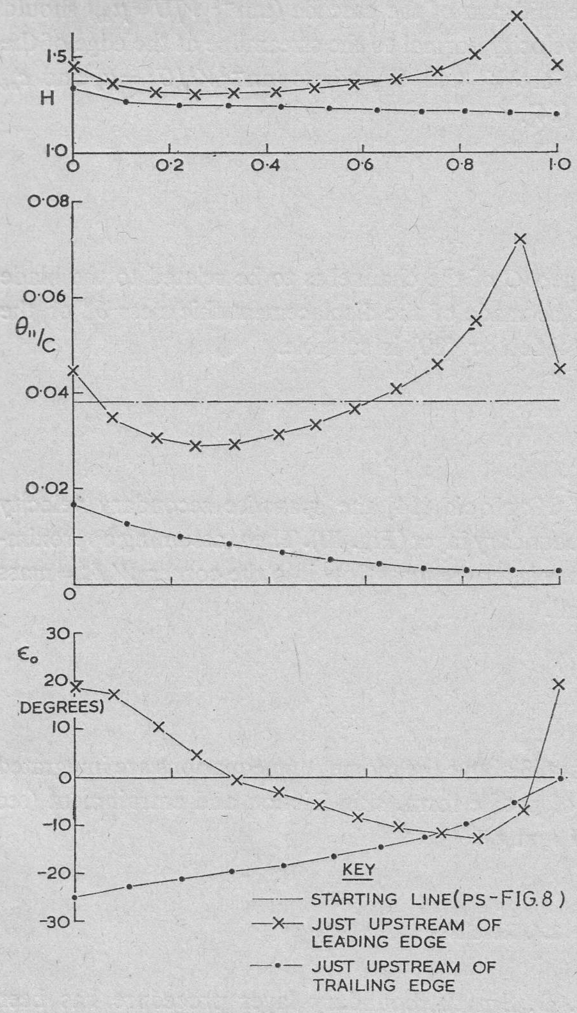

Fig. 11. Results of the three-dimensional boundary layer calculation

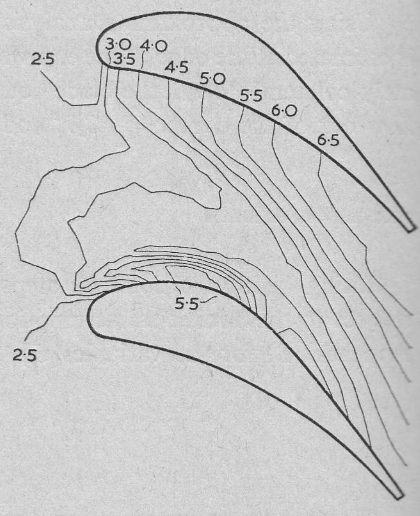

Fig. 12. Calculated distribution of skin friction coefficient on the end wall ($\times 10^3$)

This thinning of the boundary layer requires consideration of whether relaminarization might take place. The criteria quoted in [16] are:

(a) shape factor $H=\delta_1^*/\Theta_{11}$ should be less than 1.3,

(b) $$\frac{v}{C_s^2}\frac{\partial c_s}{\partial s}>2.5\times 10^{-6}\,.$$

In this particular case these are not satisfied anywhere in the flow field.

Figure 12 shows the calculated distribution of skin friction coefficient on the end-wall. The local maximum on the suction side of the passage is a result of the acceleration of the boundary layer there before thickening has taken place due to secondary flow.

The overall enhancement of the skin friction is the result of the thinning of the boundary layer and the direction of the contours at exit from the blade is strongly influenced by the skew there.

It should be noted that the calculated value of H (shape factor) varies quite considerably over the region considered and the use of a method, where H is constant (e.g. [6]) would be questionable. In the case of an impulse blade this variation might be smaller.

3. A three-dimensional inviscid calculation method

3.1. Introduction

Both the previous methods are of limited application when the boundary layer becomes comparable with the span. However the third method which was developed by Stuart [26] and reported in its basic form by Stuart and Hetherington [27] is of general application, the main limitations being the assumption of inviscid flow and the resultion which is practical on existing computers. In general terms it can be used to study the effect of any significant geometric or aerodynamic change on the movement of the low total pressure fluid in its complex three-dimensional motion in the blade passage. Such features as the accumulation of the boundary layer downstream of the blade row can be seen in the results. A calculation of the transport of the boundary layer across the passage was performed by Ehrich and Detra [8] using a simple secondary flow analysis. However in their case no variation in the mainstream velocity could be allowed due to excessive turning of the Bernoulli surfaces, and moreover such a variation violates the assumptions leading to the secondary flow stream function. All such limitations are removed in this full finite difference form of the equations of motion.

Comparisons can, of course, be made with simplified secondary flow analyses as a check on the method and to check on the assumption of methods 1 and 2. Due to the somewhat "experimental" nature of three-dimensional calculations the solution procedure will be described in more detail and the experience gained in getting the program working and in its subsequent use will be discussed.

3.2. The method

The method is for the numerical solution of fully three-dimensional inviscid internal flows. The equations are written in general curvilinear coordinates specialized to flows which are steady relative to a cascade which may be of arbitrary shape. These calculations are performed on a fixed grid; a typical grid is shown in Fig. 13 and consists of a series of planes (usually parallel with the pitch) which contain coordinate lines *1* and *2*, and coordinate lines *3* which connect these planes. As in two space variable streamline curvature methods the equations are written in terms of one component of velocity (v) along the curvilinear coordinate *3*; (which is not a streamline, through it may be roughly streamwise). The other two components are scaled by it ($u=\lambda_1 v$, $w=\lambda_2 v$). As a result of manipulations the basic set of equations (1 continuity, 3 momentum) is replaced by the set (1 continuity, 2 momentum, 1 Bernoulli) where the momentum equations are along the coordinate lines *1* and *2*. Since either of these momentum equations can be solved for an estimate of v if λ_1 and λ_2 are known throughout the field (e.g. from a previous iteration of the solution) then two estimates of v (called $v_{(1)}, v_{(2)}$) are provided. This is the key to the solution method. To create a numerical procedure which will produce identical solutions for v from both momentum equations, a term proportional to the magnitude of their difference is introduced into the continuity equation (which can be written for either $v_{(1)}$ or $v_{(2)}$). This extra term is $\beta \cdot |v_{(2)} - v_{(1)}|$, where β is a (dimensional) number called the source-sink strength whose value is limited

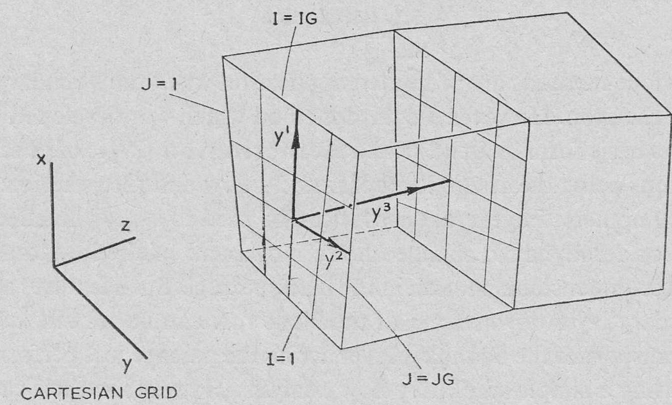

Fig. 13. Curvilinear grid showing coordinate lines

by stability considerations and has to be adjusted to obtain convergence. As the procedure converges and both momentum equations are identically satisfied the extra terms tend to zero and the continuity equation is also satisfied.

A general limitation is that the equations are singular if v is zero. Thus stagnation points are singularities and cannot be reproduced and recirculations are excluded. The basic equations and a further description of the method of solution are contained in Appendix C. In short, after manipulation the equations are written in terms of the variables $v_{(1)}, v_{(2)} M^2$ (M is the Mach No.), $\lambda_1, \lambda_2, H_0$ (the stagnation enthalpy) $A = e^{-s}/g^{JC} v$ (entropy function), and the solution proceeds iteratively after the geometry of the cascade has been worked out and the various relaxation factors specified.

3.3. Practical considerations

For stability reasons some of the various quantities ($v_{(1)}, v_{(2)}, H_0, A$) are related against their previous values as the solution proceeds. These relaxation factors must be specified in addition to the source-sink strength β. Also, in a cascade solution a repeat boundary condition factor (α) (see Appendix)must be specified. Guidance for these is obtained from the stability analysis of Stuart [26] and the factors are automatically scaled accordingly. Thus the numbers which are specified in the range]0, 1[. Further variation is necessary as both β and α have an important effect on the ability to converge. In practice it is found that the values of the relaxation factors for $v_{(1)}, v_{(2)}, H_0$ and A are not too critical.

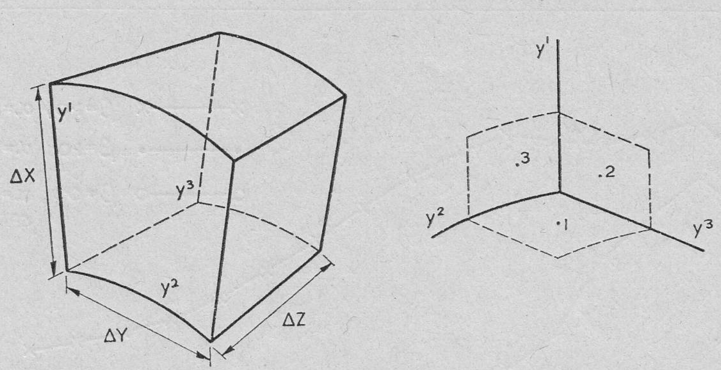

Fig. 14. Unit curvilinear cube showing aspect ratios and storage of variables

In general, like two-dimensional streamline curvature methods convergence is not good for high grid aspect ratios i.e. when $\Delta x/\Delta z$ or $\Delta y/\Delta z$ is large (Fig. 14). Since Δz can only be increased by reducing the number of computing planes and hence the attainable accuracy, and Δx or Δy can only be reduced at the expense of increased storage and computing time, there is a limit on the pitch and span of a cascade which can be easily computed. The factors which make the solution more difficult (i.e. more iterations required, more care required in choosing the values of α and β) are:

(a) the grid aspect ratio, normally related to the cascade aspect ratio (space/chord);

(b) the distortion of the grid which may be required in order to resolve a thin boundary layer;

(c) the degree of non-uinformity of the inlet flow.

The worse these factors are, the lower α and β must be and computing times to convergence are correspondly increased. These are:

(a) the root mean square difference between $v_{(1)}$ and $v_{(2)}$ at any given iteration (RMS). This is a measure of overall convergence.

(b) the root mean square difference between the values of λ_2 on the boundaries which should repeat (RRMS). This is a measure of the accuracy with which the cascade condition is being fulfilled. Within moderate limits α does not affect RMS though β affects both RMS and RRMS. To obtain good convergence or even any convergence at all some trial and error search with α and β was found to be necessary, and as an example the first case which was attempted will be taken.

The computer programme (in its original form) was provided by Dr. A. Stuart of R-R (1971) Ltd., and certain adaptations and alterations had to be made before it was compatible with the Cambridge computer system. The calculation which was then attempted was for a cascade of impulse turbine blades tested by Armstrong [2] with a thin and a thick inlet boundary layer. The thin inlet boundary layer case, being the more severe test, was attempted first. The span of the cascade is 18 inches and by assuming the flow to be symmetric about mid-span the spanwise size of the region to be computed is 9 inches. A grid of 9 points spanwise, 8 points pitchwise with 19 planes was chosen giving a computer storage requirement of 180 k-bytes and a time per iteration of about 3.5 seconds on an IBM 370/165. Seven planes were used within the blade row and target RMS and RRMS values were set at 1.0% and 0.08% respectively. The spacing ratio, which

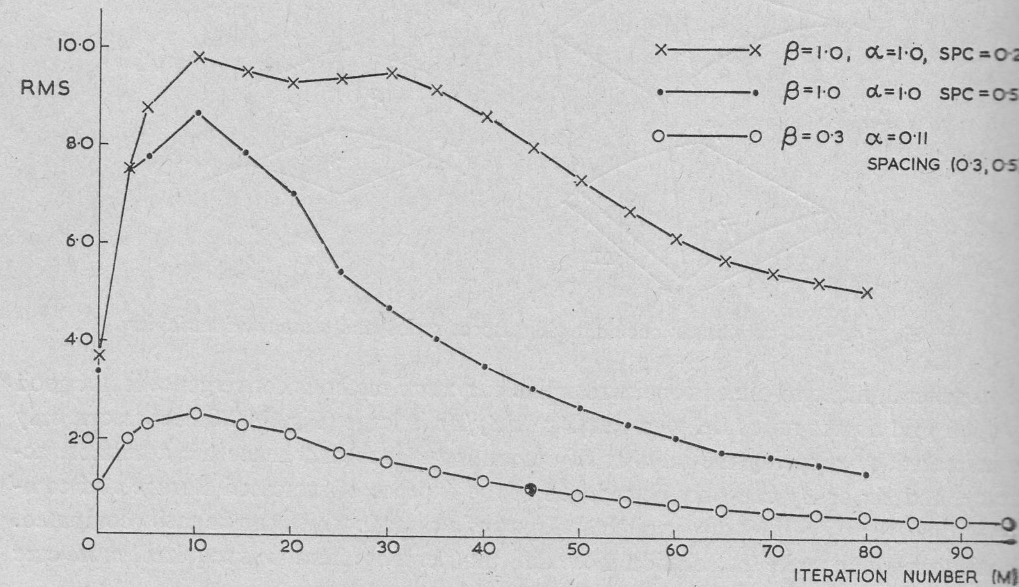

Fig. 15. Convergence behaviour of Stuart and Hetherington procedure for Armstrong cascade

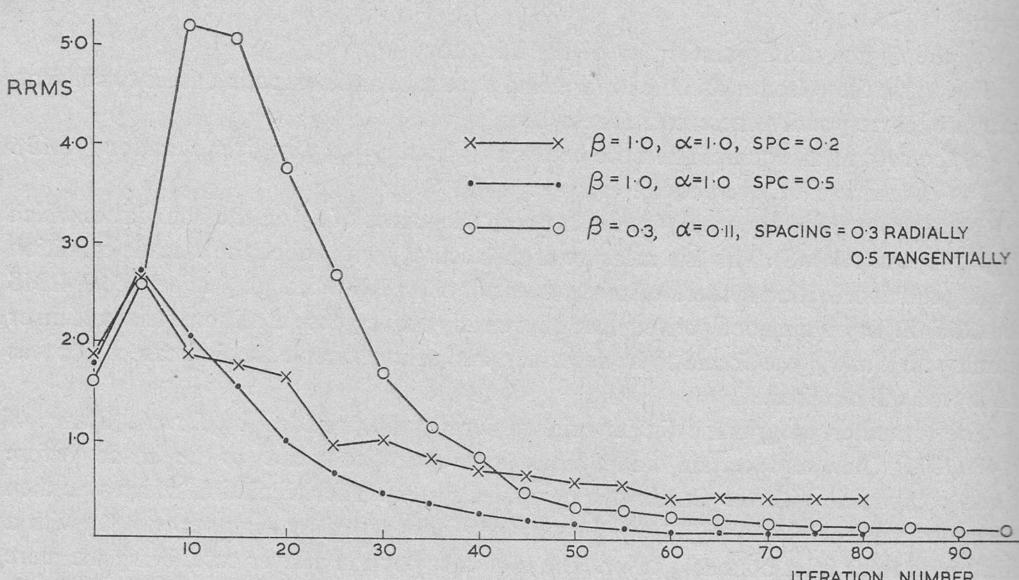

Fig. 16. Stuart and Hetherington procedure – Armstrong cascade

fixes the ratio of the smallest distance between grid points to the largest (in the $y_1 y_2$ plane) was set at 0.2. This concentrates the grid points near the walls of the blade row, providing calculation points within the (thin) boundary layer. With an α of 1.0 and a β of 1.0 the behaviour of the RMS and RRMS quantities can be seen in Figs. 15, 16. Lowering the distortion

Table 1

Results of Stuart and Hetherington procedure for 90° bend

Radius (in)	Calculated Mach No.	Free vortex Mach No.
13.22	0.1019	0.1019
13.67	0.0985	0.0985
14.11	0.0954	0.0954
14.56	0.0925	0.0925
15.00	0.0897	0.0898
15.44	0.0872	0.0872
15.89	0.0847	0.0847
16.33	0.0824	0.0824
16.78	0.0802	0.0803

of the grid by increasing the spacing ratio from 0.2→0.5 improved the convergence but had an adverse effect upon the resolution. After some more trials it became apparent that the spacing mechanism had to be altered and this was done so that different spacing ratios were possible in the spanwise and pitchwise directions. Also the type of spacing in the spanwise direction was altered so that higher values of the spacing ratio could be used and still resolve the boundary layer. Five more trials using spacing ratios of 0.3 (spanwise) and 0.5 (pitchwise) and various values of α and β then produced the desired accuracy in a computer run 96 iterations in length (see Figs. 15, 16).

3.4. Results

The results of three calculations are presented. The first is an example calculation for a simple flow; that in a duct of square cross-section with a 90 degree bend and a uniform inlet flow. The duct is 4 inches $\times 4$ inches (square), 15 inches mean radius. A $9\times 8\times 18$

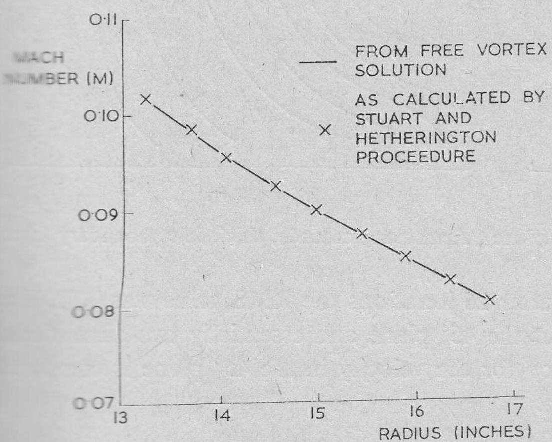

Fig. 17. Results of Stuart and Hetherington procedure for 90 degree bend

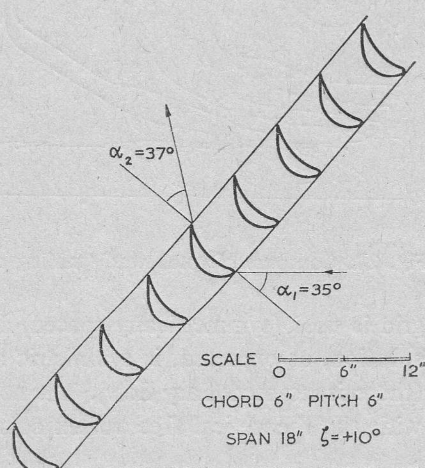

Fig. 18. Details of Armstrong cascade

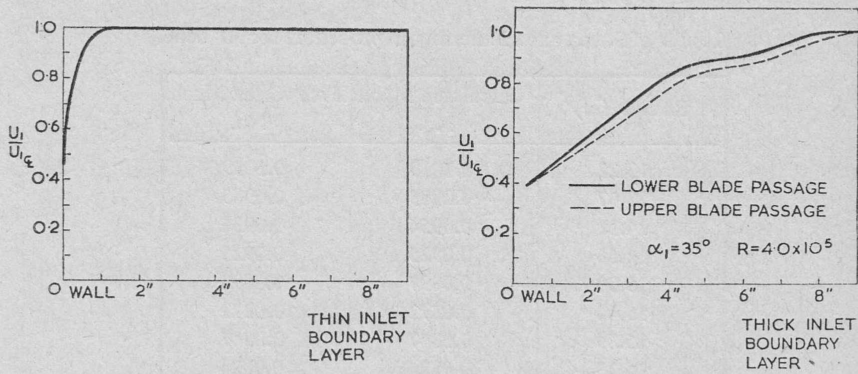

Fig. 19. Inlet boundary layer profiles, Armstrong cascade

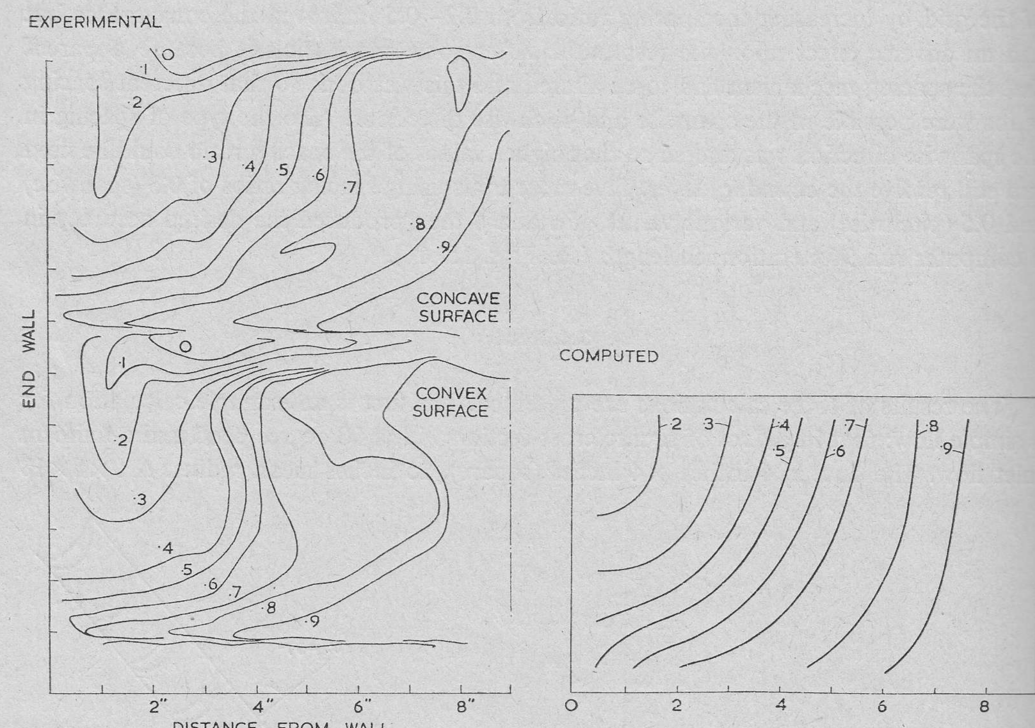

Fig. 20. Contours of total head (trailing edge plane), Armstrong cascade, thick inlet boundary layer

grid is used (symmetrically spaced) and after 25 iterations the RMS value was 0.17. The solution, as expected, is symmetric about the 45° plane and essentially two-dimensional (there is no secondary flow). The solution for the velocity in the 45° plane is compared with the theoretical free vortex solution.

$$(VR = \text{a constant}) \text{ in Figure } 17^*$$

---

* Thanks are due to Dr. A. Stuart for providing the results of this computation.

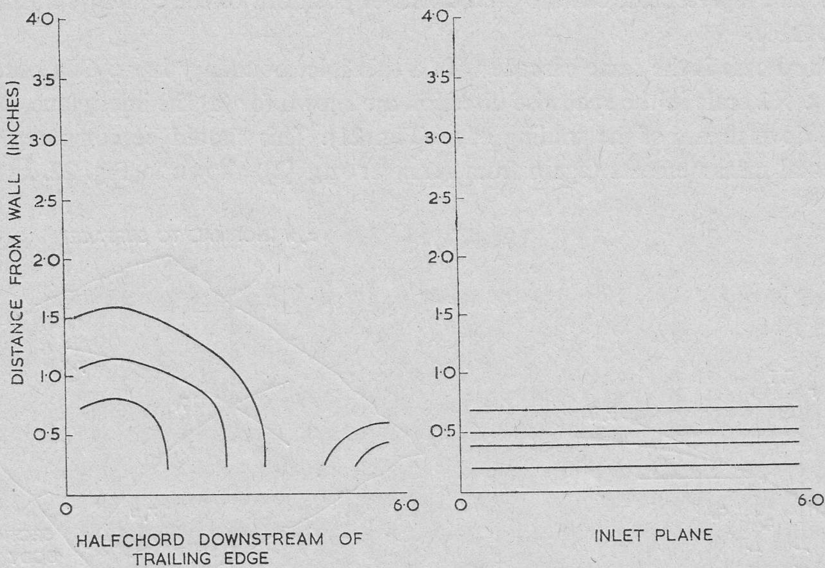

Fig. 21. Calculated contours of total head, Armstrong cascade, thin inlet boundary layer

The second case is the flow in the cascade tested by Armstrong which was mentioned above, with the thick inlet boundary layer (Figs. 18, 19).

An α of 0.08 and β of 0.20 gave convergence in 80 iterations (a spacing ratio of 1.0 was used in both directions). Contours of total head as fractions of the mid-span inlet dynamic head are shown for the trailing edge plane in Fig. 20. The latter should be compared with the experimental contours (from Armstrong [2]). The blade boundary layers are,

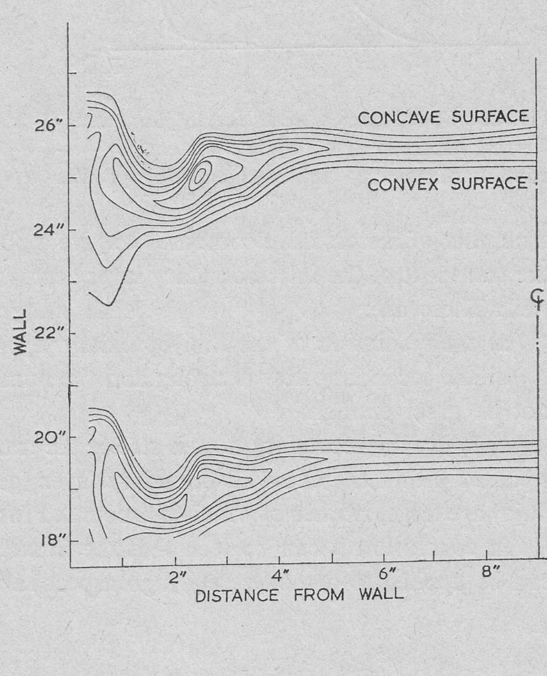

Fig. 22. Experimental contours of total head (half chord from trailing edge), Armstrong cascade, thin inlet boundary layer

of course, not represented, but the predictions of positions of the contours in the passage are reasonable.

The third case is the same cascade with a thin inlet boundary layer. Contours of total head, on a $\times 2$ scale in the spanwise direction are shown for (a) the inlet plane (b) a plane $^1/_2$ chord downstream of the trailing edge (Fig. 21). This should be compared with the experimental measurements (again from Armstrong [2]) shown in Fig. 22. In this case

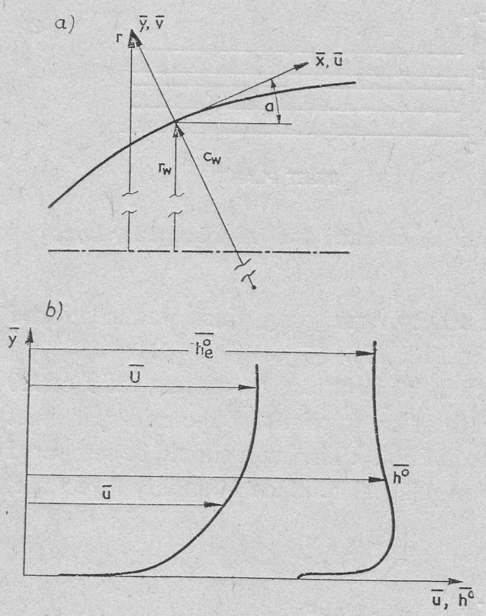

Fig. 23. Coordinate system for Mellor and Herring method; a) coordinate system, b) description of velocity and total enthalpy profiles

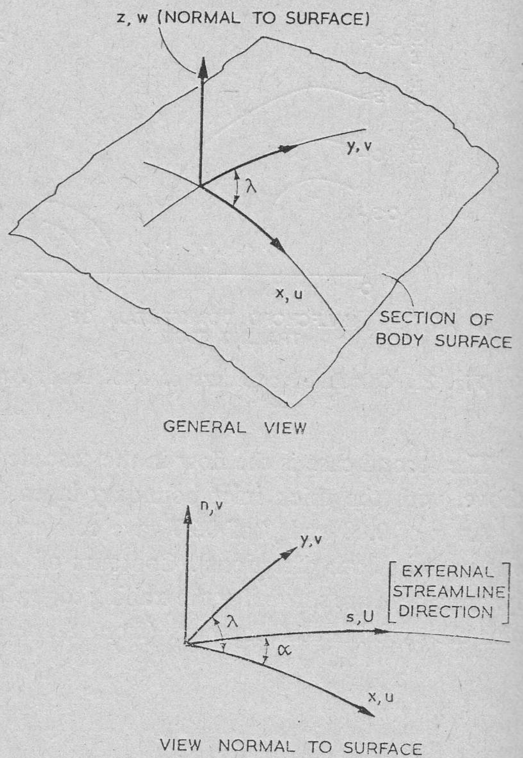

Fig. 24. Notation for three-dimensional boundary layer calculation

a number of factors have combined to give a poor comparison with experiment, although the transport of the inlet boundary layer across the passage seems to be represented quite well. These are:

a) the resolution of the thin boundary layer is not as good,

b) the secondary flow is strong and the number of planes in the stream direction may not be great enough,

c) when the secondary flow is strong the transport of blade boundary layer and dissipation within the end-wall boundary layer (generation of new low stagnation pressure fluid) are large, neither of which is accounted for in the calculation.

In conclusion it can be seen that the Stuart and Hetherington calculation procedure can be applied to a moderately high aspect ratio turbine cascade.

The results for the flow in an impulse turbine cascade with a thick inlet boundary layer compared favourably with experimental results but with a thin inlet boundary layer were not as good. Both might be improved by the inclusion of a mechanism for dissipation and work on this is in hand. The prediction for the thin inlet boundary layer might also be improved by the greater resolution permitted by larger computing grids.

Conclusions

None of the methods presented here is able to represent all aspects of the flow which takes place at blade ends. However, each of the three has its advantages and all should be capable of further development.

Of the three methods the annulus wall boundary layer theory has the most practical interest due to its speed and simplicity. However, before it can be used for large deflection turbine cascades more work is needed on the non-axisymmetric terms in the equations. The type of correlation proposed by Daneshyar [4] for the force deficit integral (D_y) may be of use though the theoretical formulation of Lindsay has better foundation.

The three-dimensional boundary layer approach avoids this problem but at the expense of extra computation. Here experimental results are needed for comparison with the calculations. Then the effect of the various physical assumptions (such as the skin friction equation) and the assumptions of the model (such as pressure transmitted through the boundary layer) could be assessed.

The third method does not make the boundary layer assumption and attacks the problem of the three-dimensional nature of the flow. However, this is achieved by discarding the (usually) turbulent, viscous nature of the end-wall region and it is of obvious importance to attempt to include these in a simple approximate way.

Acknowledgment. This work has been carried out with the support of the Procurement Executive, Ministry of Defence.

References

[1] D. G. Ainley, G. C. R. Mathieson, *An examination of the flow and pressure losses in blade rows of axial flow turbines*. ARC R.&M. 2891, 1951.
[2] W. D. Armstrong, *The secondary flow in a cascade of turbine blades*. ARC R.&M. 2979, 1957.
[3] D. E. Coles, *The law of the wake in the turbulent boundary layer*. JFMl, **2**, p. 191, 1956.
[4] M. Daneshyar, *Annulus wall boundary layers in turbomachines*. Ph. D. Thesis, Cambridge University, 1973.
[5] M. Daneshyar, J. H. Horlock, H. Marsh, *The prediction of annulus wall boundary layers in axial flow turbomachines*. NATO AGARDograph No. 164, 1972.
[6] R. P. Dring, *A momentum-integral analysis of the three-dimensional turbine end-wall boundary layer*.
[7] J. Dunham, *A review of cascade data and secondary losses in turbines*. J. Mech. Eng. Sci. **12**, 1, 1970.
[8] F. F. Ehrich, R. W. Detra, *Transport of the boundary layer in secondary flow*. JAS **21**, 1954.
[9] D. G. Gregory-Smith, *Annulus wall boundary layers in turbomachines*. Ph. D. Thesis, Cambridge University, 1970.

[10] W. R. Hawthorne, *Some formulae for the calculation of secondary flow in cascades.* ARC 17519, 1955.
[11] M. R. Head, *Entrainment in the turbulent boundary layer.* ARC R.&M. 3152, 1958.
[12] J. H. Horlock, *Axial Flow Turbines.* Butterworths, London 1966.
[13] J. H. Horlock, *Boundary layer problems in axial turbomachines.* [in] "Flow Research on Blading". ed. Dzung. Elsevier, Amsterdam 1970.
[14] J. H. Horlock, *Cross-flows in bounded three-dimensional turbulent boundary layers.* J. Mech. Eng. Sci. **15**, 4, 1973.
[15] J. H. Horlock, H. Marsh, *Wall boundary layers in turbomachines.* J. Mech. Eng. Sci. **14**, 6, 1972.
[16] J. H. Horlock, H. J. Perkins, *Annulus wall boundary layers in turbomachines.* NATO AGARDograph No. 185, 1974.
[17] J. P. Johnston, *On the three-dimensional turbulent boundary layer generated by secondary flow.* Trans. ASME **81**D (3), 1960.
[18] W. C. Lindsay, *Tip clearance effects in the growth of annulus wall boundary layers in turbomachines.* Ph.D. Thesis, Cambridge University, 1973.
[19] H. Marsh, *A digital computer program for the throughflow fluid mechanics in an arbitrary turbomachine using a matrix method.* ARC R.&M. 3509, 1966.
[20] G. L. Mellor, H. J. Herring, *A computer program to calculate laminar and turbulent boundary layer development in compressible flow with heat transfer.* NASA CR, 1973.
[21] D. F. Myring, *An integral prediction method for three dimensional turbulent boundary layers in incompressible flow.* RAE Farnborough TR 70147, August, 1970.
[22] R. A. Novak, *Streamline curvature computing procedures for fluid flow problems.* Trans. ASME **89**A, 1967.
[23] H. J. Perkins, *The turbulent corner boundary layer.* Ph. D. Thesis, Cambridge University, 1970.
[24] D. J. Smith, *Calculation of the flow past turbomachine blades.* Proc. I. Mech. E. **184**, Pt. 3G, 1970.
[25] P. D. Smith, *An integral prediction method for three-dimensional compressible turbulent boundary layers.* ARC R.&M. 3739, 1974.
[26] A. R. Stuart, *A numerical solution of the three-dimensional problem of internal aerodynamics.* Ph.D. Thesis, Aston University, 1970.
[27] A. R. Stuart, R. Hetherington, *The solution of the three variable duct flow equations.* Paper delivered to Penn. State Univ. Conference on Internal Aerodynamics, 1970.

Appendix A

The Equations of the Annulus Wall Boundary Layer Method

A.1. Passage – averaging

The passage-averaged momentum integral equations as derived in [4] and given in [15] are

$$\frac{d\Theta_{ss}}{dx}-\operatorname{tg}\mu_\delta\left[\frac{d\Theta_{sN}}{dx}+(\Theta_{ss}-\Theta_{NN})\frac{d\mu_\delta}{dx}\right]+P(2\Theta_{ss}+\delta_s^*)-Q(2\Theta_{sN}+\delta_N^*)=$$

$$=\frac{\tau_w\cos\varepsilon_0\cos\mu_\delta}{\rho C_x^2}+\frac{D_y\sin 2\mu_\delta}{2C_x^2}+\frac{D_x\cos^2\mu_\delta}{C_x^2}, \quad \text{(A.1)}$$

$$\frac{d\Theta_{Ns}}{dx}-\operatorname{tg}\mu_\delta\left[\frac{d\Theta_{NN}}{dx}+2\Theta_{Ns}\frac{d\mu_\delta}{dx}\right]+P\,[2\Theta_{Ns}-\operatorname{tg}\mu_\delta(\Theta_{ss}-\Theta_{NN}+\delta_s^*)]+Q\,(\Theta_{ss}+\delta_s^*-\Theta_{NN})=$$

$$=\frac{\tau_w\sin\varepsilon_0\cos\mu_\delta}{\rho C_x^2}+\frac{D_y\cos^2\mu_\delta}{C_x^2}-\frac{D_x\sin 2\mu_\delta}{C_x^2}, \quad \text{(A.2)}$$

where $D_x = D_{x_1} + D_{x_2} + D_{x_3}$, $D_y = D_{y_1} + D_{y_2}$

$$D_{x_1} = \int_0^{\delta} \left(\frac{F_y \operatorname{tg} \beta - f_y \operatorname{tg} \beta}{\rho} \right) dz,$$

$$D_{x_2} = \int_0^{\delta} \frac{\partial}{\partial x} (\overline{C_x'^2} - \overline{c_x'^2})\, dz,$$

$$D_{x_3} = \frac{1}{\rho} \int_0^{\delta} \left[\left(\frac{d\bar{p}}{dx} \right) - \left(\overline{\frac{\partial p}{\partial x}} \right) \right] dz,$$

and $f_y = (p_a - p_b)/(b - a)$ etc.

$$D_{y_1} = -\int_0^{\delta} \left(\frac{F_y - f_y}{\rho} \right) dz,$$

$$D_{y_2} = \int_0^{\delta} \frac{\partial}{\partial x} (\overline{C_x' C_y'} - \overline{c_x' c_y'})\, dz.$$

From secondary flow theory $D_x = D_{x_1} + D_{x_2} + D_{x_3} = 0$ and we assume $D_{y_2} = 0$, and from the analysis of [18]

$$D_{y_1} = \overline{C_x^2}\, 4\sqrt{3} \left(\frac{k\delta}{g \cos \mu_\delta} \right) \delta_s^* \left(\frac{8}{15}\, \delta - \delta_s^* \right) \sec^2 \mu_\delta \frac{d\mu_\delta}{dx}$$

if we take the cross-flow referred to the flow direction at $z = \delta$ (defined as $p_0 = $ constant) and μ_δ is known by experiment or

$$D_{y_1} = \overline{C_x^2} (2\delta - \delta^*) \frac{4\sqrt{3}\delta_s^*}{g \cos \mu_\infty} \sec^2 \mu_\infty \frac{d\mu_\infty}{dx},$$

where μ_∞ is known from analysis and μ_δ can be calculated using

$$c_{N\delta} = -C_s 2\sqrt{3}\, \delta_s^* e^{-(k\delta/g \cos \mu_\infty)}.$$

A.2. Profile assumptions

Coles profile:

$$\frac{c_s}{c_\tau} = \frac{1}{0.4} \ln \left(\frac{c_\tau z}{\nu} \right) + \frac{\pi}{0.4} W \left(\frac{z}{\delta} \right) + 5.5,$$

where $W(z/\delta) = (1 - \cos \pi z/\delta)$ and $c_\tau = \sqrt{\tau_w/\rho}$.

Cross-flow profile (Fig. 3):

$$\frac{\bar{c}_N}{C_s} = \operatorname{tg} \varepsilon_0, \qquad z < z_p$$

$$\bar{c}_N = A(C_s - c_s) + c_{N\delta} e^{k(\delta - z)}, \qquad z > z_p$$

where $k = \dfrac{\sqrt{12}}{g \cos \mu}$, $\quad c_{N\delta} = -2\sqrt{3}\, \dfrac{A C_s \delta_s^* e^{-k\delta}}{g \cos \mu_\delta}$.

[This reduces to $c_N/C_s = A(1 - c_s/C_s)$, the Johnston profile, as $\delta/g \cos \mu_\delta \to 0$].

From secondary flow analysis

$$A = A_{\text{inlet}} + A', \text{ where } A' = 2C_s^2 \int_{\mu_1}^{\mu_2} \frac{d\mu}{C_s^2}.$$

Then an equation is formed for z_p from the definition of the crosswise and streamwise profiles at $z = z_p$, which is differentiated to obtain

$$\frac{d}{dx}\left[\frac{\omega}{0.4}\ln\left(\frac{z_p\omega C_s}{\nu}\right)\right] + \frac{d}{dx}\left[\frac{\Pi\omega}{0.4}W\left(\frac{z_p}{\delta}\right)\right] + A\frac{d\omega}{dx} = \frac{d}{dx}\left[\frac{A}{A+\operatorname{tg}\varepsilon_0}\right] + \frac{d}{dx}\left[\frac{c_{N\delta}\,e^{k(\delta - z_p)}}{C_s(A+\operatorname{tg}\varepsilon_0)}\right]. \tag{A.3}$$

A.3. Other assumptions

Skin frictions: $\omega = f_1(H_s, Re_\theta) = f_2(\Pi, Re_\delta)$ by assumption: $1/\omega = ln\omega/0.4 + (1/0.4)\ln(Re_\delta) + 2\Pi/0.4 + 5.5$ from the Coles profile at $z = \delta$ this can be differentiated and written

$$\frac{1}{\delta}\frac{d\delta}{dx} + \frac{2d\Pi}{dx} + \left(\frac{1}{\omega} + \frac{0.4}{\omega^2}\right)\frac{d\omega}{dx} + \frac{1}{C_s}\frac{dC_s}{dx} = 0. \tag{A.4}$$

Entrainment:

$$E = \frac{1}{C_s}\frac{d}{ds}\left[C_s(\delta - \delta_s^*)\right] = E(H_E) = E\left(\frac{\delta - \delta_s^*}{\Theta_{ss}}\right) \simeq 0.0306(H_E - 3)^{-0.653}$$

or

$$\frac{d}{dx}(\delta - \delta_s^*) + \operatorname{tg}\mu_\delta \frac{d\delta_N^*}{dx} = \frac{1}{\cos\mu_\delta}E(H_E) - \frac{(\delta - \delta_s^*)}{C_x}\frac{dC_s}{dx} - Q\delta_N^*. \tag{A.5}$$

Equations (A.1), (A.2), (A.3), (A.4) and (A.5) are the five equations which are solved for $(\delta, \Pi, \varepsilon_0, z_p, \omega)$.

Appendix B

The Equations used in the Three-Dimensional Boundary Layer Procedure

B.1. Blade to blade potential flow

Ref. [24] describes a method to solve the inviscid blade-to-blade flow. The equations used are those for steady, reversible flow in relative framework.

Continuity:

$$\nabla \cdot (\rho W) = 0,$$

Momentum:

$$2\Omega \times W - W \times (\nabla \times W) = \nabla I - T\nabla S,$$

Energy:

$$\frac{DI}{Dt} = 0,$$

Entropy:

$$T\frac{DS}{Dt} = Q.$$

State (perfect gas)

$$\rho = \rho(h, s) = A^{\frac{1}{\gamma - 1}} h e^{-\frac{s}{R}}.$$

These equations are solved in finite difference form by a band matrix method. The output is values of the velocities at all grid points.

B.2. Blade boundary layer solution

The equations to be solved, for the compressible two-dimensional boundary layer are (see Fig. 23)
Continuity:

$$\frac{\partial}{\partial \bar{x}}(\rho r \bar{u})+\frac{\partial}{\partial \bar{y}}(r \overline{\rho v})=0 .$$

Momentum:

$$\overline{\rho u}\frac{\partial \bar{u}}{\partial \bar{x}}+\overline{\rho v}\frac{\partial \bar{u}}{\partial \bar{y}}=\rho_e U\frac{dU}{dx}+\frac{1}{r}\frac{\partial (r\bar{\tau})}{\partial \bar{y}} .$$

Energy:

$$\overline{\rho u}\frac{\partial \bar{h}_0}{\partial \bar{x}}+\overline{\rho v}\frac{\partial \bar{h}_0}{\partial \bar{y}}=-\frac{1}{r}\frac{\partial}{\partial \bar{y}}[r(\bar{q}+\bar{u}\bar{\tau})],$$

where $r(\bar{x}, \bar{y})=r_w(\bar{x})+\bar{y}(\cos\alpha(x))$; lower case letters denote values within the boundary layer and

$$\frac{\bar{\tau}}{\bar{\rho}}\equiv \nu_e\frac{\partial \bar{u}}{\partial \bar{y}}, \qquad \frac{\bar{q}}{\bar{\rho}}\equiv \nu_{eg}\frac{\partial \bar{h}}{\partial \bar{y}},$$

where

$$\nu_e=\nu_e\left(\frac{\bar{u}_\tau}{U}, Re_{\delta *}\right), \qquad \nu_{eg}=\nu_{eg}(\nu_e, Pr_T),$$

ν_e=effective viscosity, ν_{eg}=effective conductivity which assume their laminar values in a laminar flow. These equations are solved on a finite difference grid using an implicit numerical scheme.

B.3. Secondary flow velocity

A brief account of the analysis of [14] is given. Assuming the following profiles for the secondary velocities

$$W=\frac{W_s(y)\,s}{s'}, \qquad V=\frac{V_s(y)}{2s'^2}\left[\frac{s'^2}{4}-s^2\right]$$

(where s is the distance from the passage centreline, $s'=(b-a)$, Fig. 1) and satisfying continuity and the vorticity equation $\xi_s=A\dfrac{du}{dy}$ averaged across the pitch an expression for $W_{s\delta}$ (where W_s is the spanwise velocity component) can be obtained:

$$W_{s\delta}=-\frac{6AU}{s'}\left[\frac{e^{k(\delta-L)}-e^{-k\delta}}{1-e^{-kL}}\right][I_1(\delta)+I_2(\delta)],$$

where

$$I_1(\delta)=\int_0^\delta\left(1-\frac{u}{U}\right)e^{ky}dy, \qquad I_2(\delta)=\int_0^\delta\left(1-\frac{u}{U}\right)e^{-ky}dy,$$

$$k=\sqrt{\frac{12}{s'}}, \qquad W_e=\frac{W_{s\delta}}{2}$$

as $L\to\infty$ and $k\delta=\sqrt{12}\,\delta/s'$ is small $e^{-k\delta}\to 1-k\delta$ and $W_{\text{wall}}(\delta)=W_e=-12AU\delta^* k\delta/s'$.

B.4. Three-dimensional boundary layer calculation

The coordinate system used is shown in Figure 24 and a typical calculation region in Figure 8. The momentum integral equations for the compressible (turbulent) boundary layer in general coordinate are [25]

$$\frac{1}{h_1}\frac{\partial \Theta_{11}}{\partial x}+\Theta_{11}\left[\frac{(2-M^2)}{h_1}\frac{1}{U_e}\frac{\partial U_e}{\partial x}+\frac{1}{q}\frac{\partial}{\partial x}\left(\frac{q}{h_1}\right)+k_1\right]+\frac{1}{h_2}\frac{\partial \Theta_{12}}{\partial y}$$
$$+\Theta_{12}\left[\frac{(2-M^2)}{h_2}\frac{1}{U_e}\frac{\partial U_e}{\partial y}+\frac{1}{q}\frac{\partial}{\partial y}\left(\frac{q}{h_2}\right)+k_3\right]+\Delta_1\left[\frac{1}{h_1 U_e}\frac{\partial U_1}{\partial x}+\frac{kU_1}{U_e}\right]$$
$$+\Delta_2\left[\frac{1}{h_2 U_e}\frac{\partial U_1}{\partial y}+\frac{k_2 V_1}{U_e}+\frac{k_3 U_1}{U_e}\right]+\Theta_{22}k_2=\frac{c_{f1}}{2},$$

$$\frac{1}{h_1}\frac{\partial \Theta_{21}}{\partial x}+\Theta_{21}\left[\frac{(2-M^2)}{h_1}\frac{1}{U_e}\frac{\partial U_e}{\partial x}+\frac{1}{q}\frac{\partial}{\partial x}\left(\frac{q}{h_1}\right)+l_3\right]+\frac{1}{h^2}\frac{\partial \Theta_{22}}{\partial y}$$
$$+\Theta_{22}\left[\frac{(2-M^2)}{h_2 U_e}\frac{\partial U_e}{\partial y}+\frac{1}{q}\frac{\partial}{\partial y}\left(\frac{q}{h_2}\right)+l_2\right]+\Delta_1\left[\frac{1}{h_1 U_e}\frac{\partial V_1}{\partial x}+\frac{l_1 U_1}{U_e}+\frac{l_3 V_1}{U_e}\right]$$
$$+\Delta_2\left[\frac{1}{h_2 U_e}\frac{\partial V_1}{\partial y}+\frac{l_2 V_1}{U_e}\right]+\Theta_{11}l_1=\frac{c_{f2}}{2},$$

where the quantities k_i, l_i are functions of the metric coefficients of the coordinate system used.

In the method these equations are used together with the following empirical assumptions

a) streamwise velocity profile (Spence)

$$\frac{c_s}{C_s}=\left(\frac{z}{z_\delta}\right)^N,$$

$N=N(\bar{H})$ in incompressible flow $z/z_\delta=z/\delta$ and $H=\delta_1^*/\Theta_{11}$,

b) crosswise velocity profile (Mager)

$$\frac{c_N}{C_s}=\left(1-\frac{z}{\delta}\right)^2 \operatorname{tg}\varepsilon_0,$$

c) skin friction (along ε_0 to streamline) (Ludwieg-Tillman)

$$c_f=0.264(Re_\Theta)^{-0.268},$$

d) entrainment function $F=0.025\,\bar{H}-0.022$, where $\bar{H}$ is the transformed (compressible) shape parameter.

Thus three equations are written for the variables Θ_{11}, $\bar{H}$, ε_0 which are hyperbolic in nature. They are integrated in the x direction (Fig. 24). Derivatives in the x-direction are taken at the mid point of the step (implicit) and y derivatives are evaluated explicitly with the direction depending on the limiting characteristic disrections. The size of the x-step is determined by stability considerations.

Appendix C

The Stuart and Hetherington Three-Dimensional Inviscid Procedure

C.1. Basic equations (in cartesian tensors)

Continuity:

$$u^i_{,i}+\frac{1}{\rho}\frac{D\rho}{Dt}=0, \tag{C.1}$$

Momentum:

$$\frac{Du^i}{Dt}+\frac{1}{\rho}p_{,i}=0 \text{ (inviscid)}, \tag{C.2}$$

Energy:

$$\frac{Ds}{Dt}=0 \text{ (inviscid and adiabatic)}, \tag{C.3}$$

State:

$$p=\rho RT \text{ (perfect gas)}, \tag{C.4}$$

$$h=c_p\, T. \tag{C.5}$$

Second law of thermodynamics:

$$\frac{dp}{\rho}=dh-T ds. \tag{C.6}$$

Here the variables u^i, p, ρ, s, T, h are functions of x^i and t where x^i is a fixed (inertial) cartesian system. Now consider the curvilinear coordinates $y^i=y^i(x^i, t)$ (an inverse is assumed). These co-ordinates are chosen so that the boundaries of the computing region are coordinate planes (e.g. $y_1=$constant, $y_2=$constant) and the choice is limited to those that rotate about a fixed axis with a constant angular velocity. Using the transformation, introducing the source-sink term into the continuity equation, the equations become, after some manipulations

Momentum:

$$(1-M^2)\Big[v^2\lambda^i\{(g_{jk}\lambda^j)_{,i}-(g_{ij}\lambda^j)_{,k}\}+2v\lambda^j E_{jk} + \frac{\partial}{\partial y^k}(H_0-R)-T\frac{\partial s}{\partial y^k}-\frac{1}{2}f\frac{\partial}{\partial y^k}(v^2)\Big]-v^2 g_{lk}\lambda^l\Big[\frac{1}{\sqrt{g}}(\sqrt{g}\lambda^i)_{,i} - \frac{1}{2}\frac{v^2}{c^2}\lambda^i f_{,i}+\frac{\lambda^i}{c^2}R_{,i}\Big]=0,$$

$$k=1: \text{(C.7)}$$
$$k=2: \text{(C.8)}$$

Continuity:

$$(\rho^{v(1)}\sqrt{g}\,v(1)\lambda^1)_{,1}+(\rho^{v(2)}\sqrt{g}\,v(2)\lambda^2)_{,2}+(\rho^{v(2)}\sqrt{g}\,v(1))_{,3} =\beta(\rho^{v(1)}v(1)\sqrt{g}-\rho^{v(2)}v(2)\sqrt{g}), \tag{C.9}$$

$$(\rho^{v(1)}v(1)\sqrt{g}\,\lambda^1)_{,1}+(\rho^{v(2)}v(2)\sqrt{g}\,\lambda^2)_{,2}+(\rho^{v(2)}\sqrt{g}\,v(2))_{,3} =\beta(\rho^{v(2)}v(2)\sqrt{g}-\rho^{v(1)}\sqrt{g}\,v(1)). \tag{C.10}$$

Energy:

$$\frac{Ds}{Dt}=0, \tag{C.11}$$

Bernoulli:

$$\frac{D}{Dt}(H_0-\tfrac{1}{2}r^2\Omega^2)=0, \tag{C.12}$$

where $v(1)$ is the solution to (C.7) and $\rho^{v(1)}$ is the associated density distribution, $v(2)$ is the solution to (C.8) and $\rho^{v(2)}$ its associated density distribution

$$v\lambda^i=v^i \quad\text{and}\quad \lambda^3=1,$$

$$R=\tfrac{1}{2}r^2\Omega^2, \quad c^2=\left(\frac{\partial p}{\partial \rho}\right)_s, \quad f=g_{ij}\lambda^i\lambda^j,$$

$$g_{jk}=\frac{\partial x^i}{\partial y^j}\frac{\partial x^i}{\partial y^k} \quad \text{(the relationship between the co-ordinate systems)},$$

$$g=|g_{ij}|=\left|\frac{\partial x_i}{\partial y^j}\right|^2.$$

These equations can be solved in turn as follows; all the other quantities being kept constant during each integration

using λ_1, λ_2 : (C.7) is integrated for $v(1)$ along all lines $y^2=$constant, $y^3=$constant,
using λ_1, λ_2 : (C.8) is integrated for $v(2)$ along lines $y^1=$constant, $y^3=$constant,
using $v(1), v(2), \lambda$: (C.9) is integrated for λ_1 along all lines $y^2=$constant, $y^3=$constant,
using $v(1), v(2), \lambda$: (C.10) is integrated for λ_2 along all lines $y^1=$constant, $y^3=$constant

subject to the boundary conditions on $v(1)$ and $v(2)$

$$\int_0^{IG} \rho_N^{v(1)} \sqrt{g}\, v_N(1)\, dy^1 = \int_0^{IG} \rho_{N-1}^{v(2)} \sqrt{g}\, v_{N-1}(2)\, dy^1 , \tag{C.13}$$

$$\int_0^{JG} \rho_N^{v(2)} \sqrt{g}\, v_N(2)\, dy^2 = \int_0^{JG} \rho_N^{v(1)} \sqrt{g}\, v_N(1)\, dy^2 , \tag{C.14}$$

where the subscript n refers to the interaction number n and the walls are specified by $y_1=0$, IG; $y_2=0$, JG (Fig. 13). The boundary conditions for λ^1 and λ^2 are $\lambda^1=0$ at $y^1=0$, IG; $\lambda^2=0$ at $y^2=0$, JG (walls) or if a repeat (cascade) condition is being applied an additional iteration is used to compute the value of λ_2 at the boundary:

$$\frac{\partial \lambda_N^2}{\partial y^3} = \frac{\partial \lambda_{N-1}^2}{\partial y^3} + \alpha (v_{LN} - v_{RN}),$$

where v_{LN} – velocity at boundary approaching from left
v_{RN} – velocity at boundary approaching from right $\Big\}$ N^{th} itn

and α is the repeat boundary condition factor; an adjustable constant whose value is so chosen that convergence is obtained.

C.2. Method of solution

The variables ($\bar{v}(1), \bar{v}(2), M^2, \lambda^1, \lambda^2, H_0, A$) where $\bar{v}(1)=\rho\sqrt{g}\,v(1)$ and similarly for $\bar{v}(2)$ are stored at the centre of the faces of the unit cube in the curvilinear coordinate system in the following manner (see Fig. 14).

At points *1* : $\lambda^1, g_{11}, g_{21}, g_{31}, \sqrt{g}$,
At points *2* : $\lambda^2, g_{12}, g_{22}, g_{32}, \sqrt{g}$,
At points *3* : $v(1), v(2), M^2, H_0, A, g_{33}, \sqrt{g}, R$.

With this storing arrangement the next important derivatives can be expressed simply in first order centred finite differences and the boundary conditions can be applied directly without calculating derivatives normal to the surfaces. The momentum equations (C.7), (C.8) written in finite difference form, are solved for $v(1)$ or $v(2)$ starting from an estimate of the velocity at the mid-point of the line along which the equation is being integrated. If the boundary condition (C.13), (C.14) is not satisfied, the velocity at the mid-point is adjusted. The most up-to-date value is always used and for stability reasons new values are always relaxed e.g. $\bar{v}_N(1)=r_{v(1)}\bar{v}_{Ni}(1)+(1-r_{v(1)})\,\bar{v}_{N-1}(1)$, where $r_{v(1)}$ is the relaxation factor for $v(1)$, $\bar{v}_N(1)$ the solution at the N^{th} iteration and $\bar{v}(1)_{Ni}$ the initial (unrelaxed) estimate. Similar relaxation factors are used for $\bar{v}(2)$, A and H_0. These vary with the grid shape and size, being scaled according to the results of the stability analysis.

N.B. the boundary conditions, as stated in (C.13), (C.14) apply to $\bar{v}(1)_N$ not $\bar{v}(1)_{NI}$ and hence for $\bar{v}(1)_{NI}$ we can write

$$\int_0^{JG} \bar{v}_{NJ}(1)\, dy^1 = \frac{1}{r_{v(1)}} \int_0^{JG} [\bar{v}_{N-1}(2) - (1-r_{v(1)})\,\bar{v}_{N-1}(1)]\, dy^1 .$$

The far downstream boundary condition applied to the momentum equation is $\partial v(1)/\partial y^3 = \partial v(2)/\partial y^3 = 0$. This is correct for the secondary flow approximation and is used in lieu of a better idea in all cases. In practice the downstream boundary layer appears only to affect the last few planes of the solution.

The continuity equations (C.9), (C.10) are integrated for λ^1 and λ^2 along the lines (y^2, y^3) and (y^1, y^3) using the fixed or repeat boundary condition as appropriate. The equation for the stagnation enthalpy and entropy are solved by tracing streamlines back to the initial plane and interpolating there, using a linear interpolation. This prevents values creeping into the solution which are outside the initial range but to prevent degradation of gradients this cannot be done in every plane.

Obliczanie przepływu przyściennego w palisadach turbin

Streszczenie

Artykuł dotyczy zastosowania trzech metod obliczania przepływu przyściennego w palisadach turbin. Każdą z metod opisano, omówiono jej założenia i, tam gdzie możliwe, podano przykładowe obliczenia i porównano ich wyniki z doświadczeniem.

W pierwszych dwóch metodach, wykorzystujących klasyczne podejście, polegające na podziale przepływu na nielepki strumień główny i warstwę przyścienną, oblicza się rozwój warstwy przyściennej dla znanego przepływu głównego. W trzeciej metodzie prowadzi się obliczenia dla całego pola przepływu.

Pierwsza metoda, metoda warstwy przyściennej przy ścianie pierścieniowej, została rozwinięta na Uniwersytecie w Cambridge w odniesieniu do palisad z małym odchyleniem; w artykule podaje się jej krótki opis, wraz z obliczeniami dla łopatki kierowniczej i akcyjnej palisady turbinowej.

Druga metoda, pochodząca od metody trójwymiarowej warstwy przyściennej dla przepływów nieograniczonych i opracowana w Royal Aircraft Establishment, Bedford, została przystosowana dla przypadku ograniczonej warstwy przyściennej w układzie łopatkowym. Omówiono jej zastosowanie dla palisady łopatkowej kierownicy w turbinie.

Metoda trzecia, obliczeń trójwymiarowego nielepkiego przepływu, opracowana na Uniwersytecie w Aston, została zaadaptowana do obliczeń palisady turbiny akcyjnej o umiarkowanie dużym wydłużeniu. Opisano tę metodę i przedstawiono trudności z jej stosowaniem oraz podano niektóre wyniki obliczeń.

Расчет пристенного течения в турбинных решетках

Резюме

Статья касается применения трех методов расчета пристенного течения в турбинных решетках. Каждый из методов описывается. Обсуждаются их предположения, а в случаях, где это было возможно, приводятся примерные расчеты, а их результаты сравниваются с результатами эксперимента.

В первых двух методах используется классический подход, состоящий в том, что поток разделяется на невязкий основной поток и пристенный слой, а потом определяется развитие пристенного слоя для известного основного потока. В третьем методе расчет проводится для целого поля течения.

Первый метод, т.е. метод пристенного слоя для кольцеобразной стенки, серьезно развернут в Университете в Кембридж относительно слабо отклоняющих решеток. В статье деатся его краткое описание вместе с расчетом для направляющих лопаток и решетки активных турбинных лопаток.

Второй метод, развитый на основе трехразмерной теории пристенного слоя для неограниченных течений, разработан в Рояль Эркрафт Эстаблишмент в Бедфорде и приспособлен для случая ограниченного пристенного слоя в решетке лопаток. Обсуждается применение метода относительно решетки направляющих лопаток в турбине.

Третий метод, т.е. метод расчета трехразмерного невязкого течения, разработанный в Университете в Астон, был приспособлен для расчетов активной турбинной решетки умеренно удлиненной. Описан метод и представлены затруднения в его применении, а также некоторые результаты расчетов.